Supplementary Information

Hydrogen-bonding engineering in a 3D cyano-bridged double-perovskite ferroelastic greatly improves the phase-transition temperature

Meng-Zhen Li,‡ Zhao-Hong Chen,‡ Sheng-Qian Hu, Jun-Si Zhou, Luan-Ying Ji and Xiao-Gang Chen*

Ordered Matter Science Research Center, Nanchang University, 330031, P. R. China.

E-mail: chenxg@ncu.edu.cn.

Experimental Section

Preparation of 1. All chemicals were commercially available and were used without further purification. Ethanolamine hydrochloride (8.193 g, 84 mmol) was added to 20 ml aqueous solution of $K_3Fe(CN)_6$ (3.951 g, 12 mmol). Place the solution together with solid sodium hydroxide in a light-protected drying oven. Reddish brown block crystals of **1** were obtained at room temperature after eight days.

Preparation of 2. All chemicals were commercially available and were used without further purification. ethylamine hydrochloride (6.849 g, 84 mmol) was added to 20 ml aqueous solution of $K_3Fe(CN)_6$ (3.951 g, 12 mmol). Place the solution together with solid sodium hydroxide in a light-protected drying oven. Brownish-black block crystals of **2** were obtained at room temperature after eight days.

Single crystal X-ray crystallography. Single-crystal X-ray diffraction measurements of **1** and **2** were performed on the Rigaku XtaLAB Synergy-DW diffractometer with Cu-Kα radiation (λ = 1.54184 Å) at various temperatures. Rigaku Crystal Clear 1.3.5 was used for data collection, cell refinement, and data reduction. The structures were solved by the direct methods and refined by the full-matrix least-squares method with

the SHELX program package on the Olex2 program. All non-hydrogen atoms were refined using anisotropic thermal parameters. The positions of the hydrogen atoms were generated geometrically. The crystal data and structure refinement are summarized in Table S1. The CCDC numbers were 2285650-2285653.

Powder X-ray diffraction. Variable-temperature powder X-ray diffraction (PXRD) data were collected by using a Rigaku D/MAX 2000 PC X-ray diffraction system with Cu Kα radiation in the 2θ range of 10°-40° with a step size of 0.02°.

DSC measurements. Differential scanning calorimetry (DSC) measurements were recorded on a Perkin-Elmer Diamond DSC instrument by heating and cooling powder samples with a rate of 20 K min^{-1} in aluminum crucibles in a nitrogen atmosphere.

Dielectric measurements. The samples were made with single crystal or pressed powder pellets. Silver conductive paste deposited on the plate surfaces was used as top and bottom electrodes. Complex permittivities were measured with a TH2828A impedance analyzer over the frequency range from 500 Hz to 1 MHz. The heating and cooling rate was artificially controlled, which is about 8 K/min. For dielectric switching measurements, the response time of one dielectric switch is about 14 minutes, and the total cycle time is about 70 minutes.

Optical microscopy measurements. Optical observations were carried out using an OLYMPUS BX53-P polarizing microscope equipped with a Linkam LTS420 cooling/heating stage. The temperature was stabilized to within 1 K.

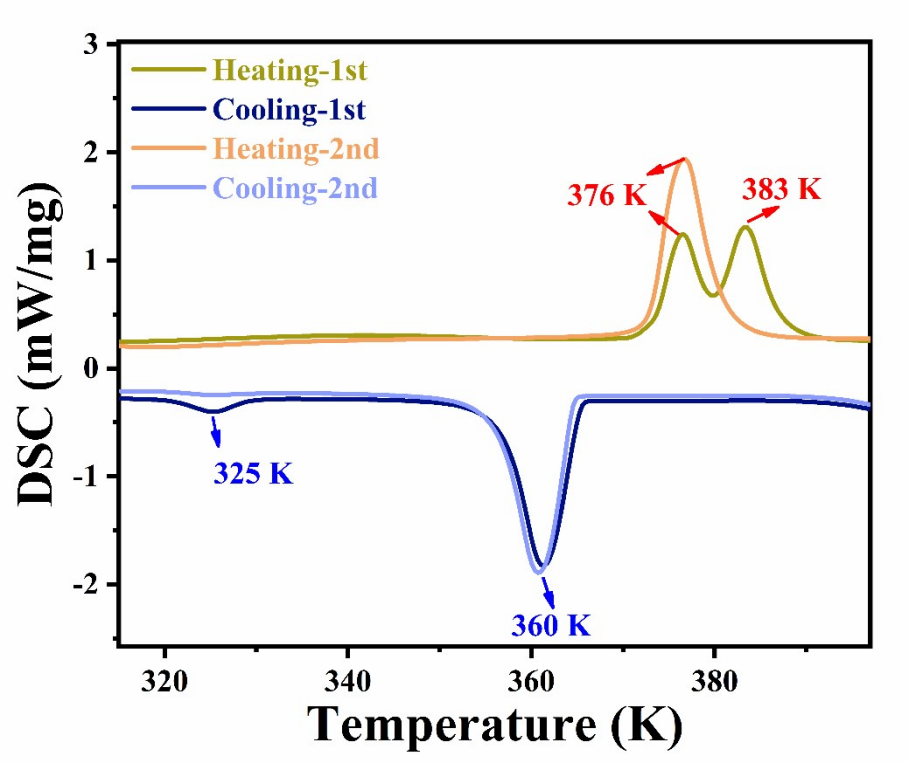

Fig. S1 DSC heating-cooling curves during different cycles (1st and 2nd) at a heating/cooling rate of 20 K/min for **1**.

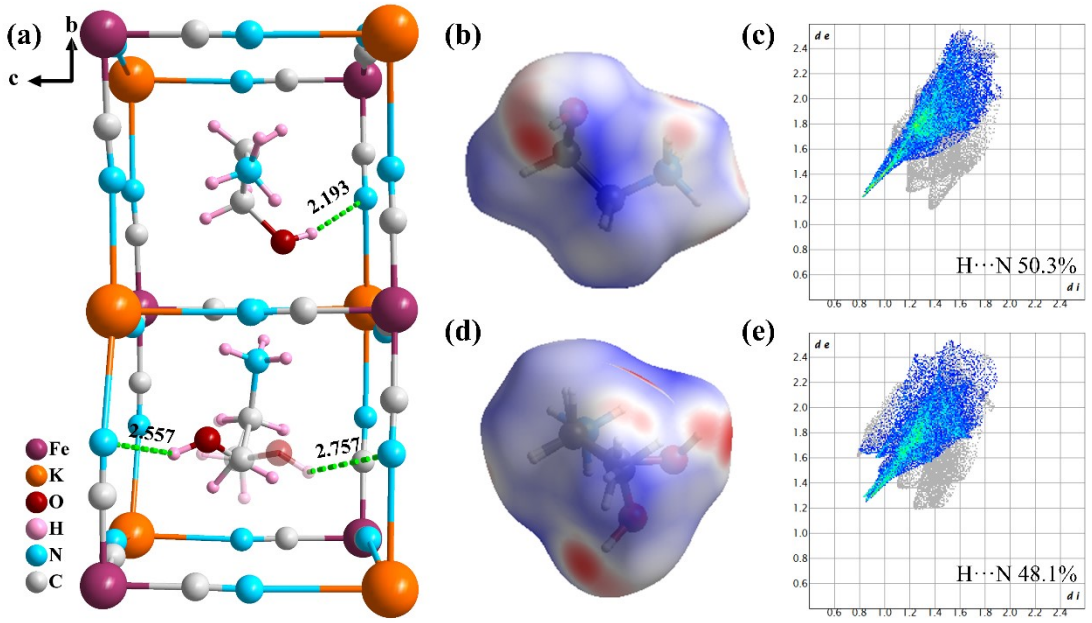

Fig. S2 (a) HBs between organic cations and framework in **1** at 300 K. The distance unit is Å. (b, c) Hirshfeld d_{norm} surfaces and 2D fingerprint plots of the ordered organic cation. (d, e) Hirshfeld d_{norm} surfaces and 2D fingerprint plots of the split organic cation.

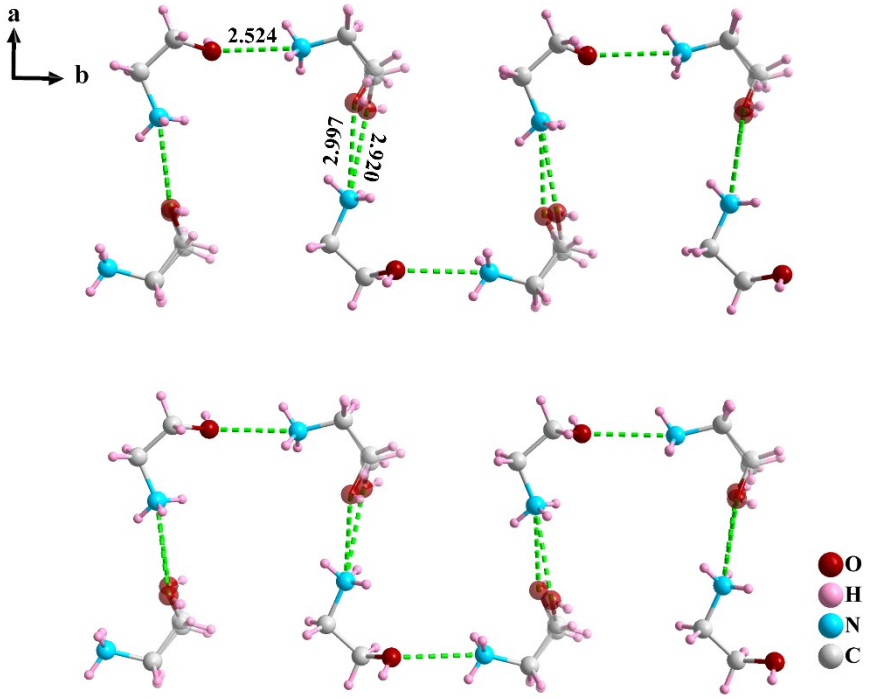

Fig. S3 One-dimensional HBs between the adjacent organic cations of **1** at 300 K along the crystallography *b*-axis. The distance unit is Å.

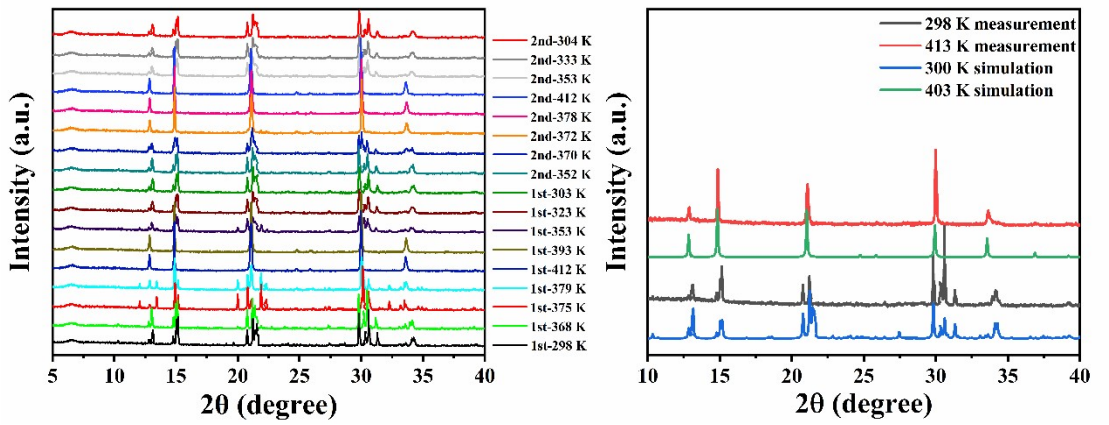

Fig. S4 (a) Measured PXRD patterns for **1** at variable temperatures in different cycles (1st and 2nd). (b) Measured and simulated PXRD patterns for **1** at variable temperatures.

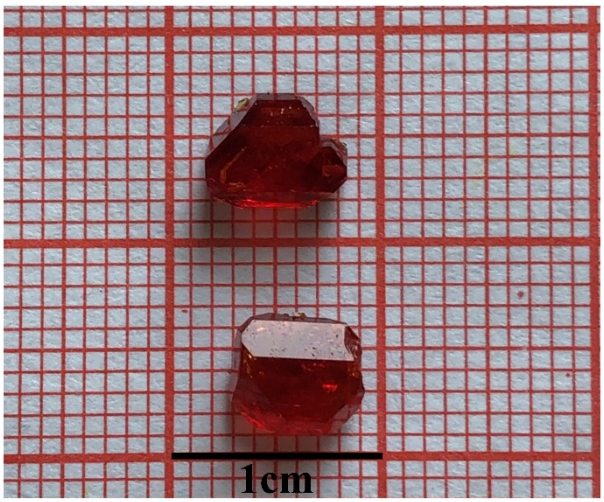

Fig. S5 Crystal morphology of **1**.

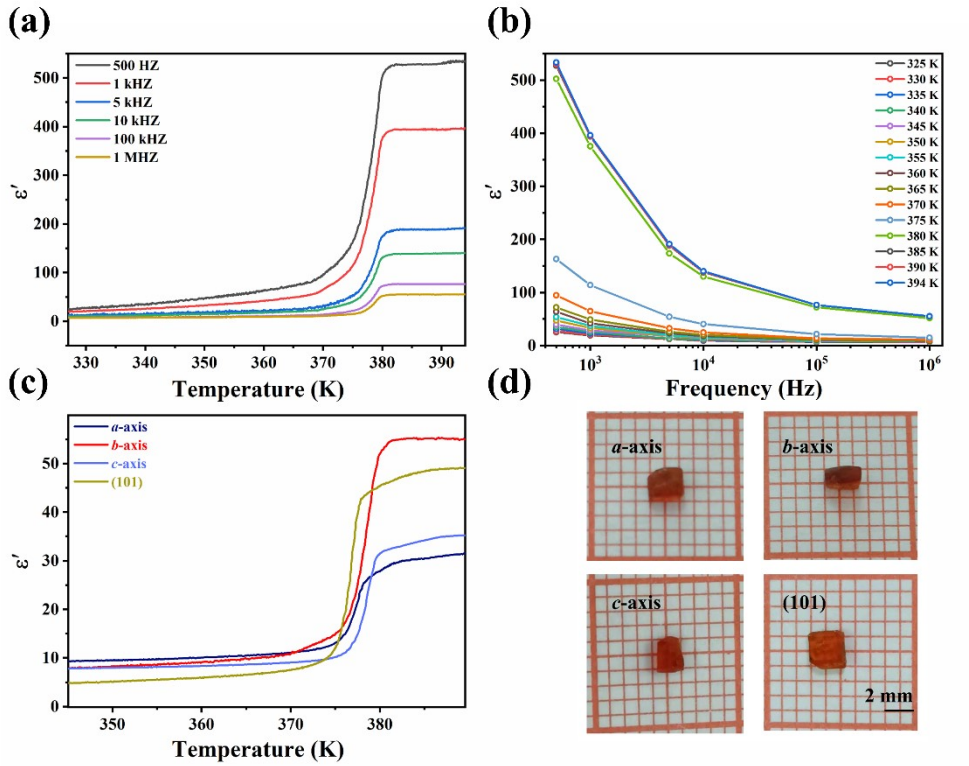

Fig. S6 (a) Temperature dependences of ε' for various frequencies for **1** along the crystallographic *b*-axis in the second heating process. (b) The frequency dependences of ε' for **1** at different temperatures along the crystallographic *b*-axis in the second heating process. (c) Temperature-dependent ε' for **1** along the crystallographic *a*-axis, *b*-axis, *c*-axis, and (101) plane measured at 1 MHz. (d) Crystal morphologies of **1** at different directions.

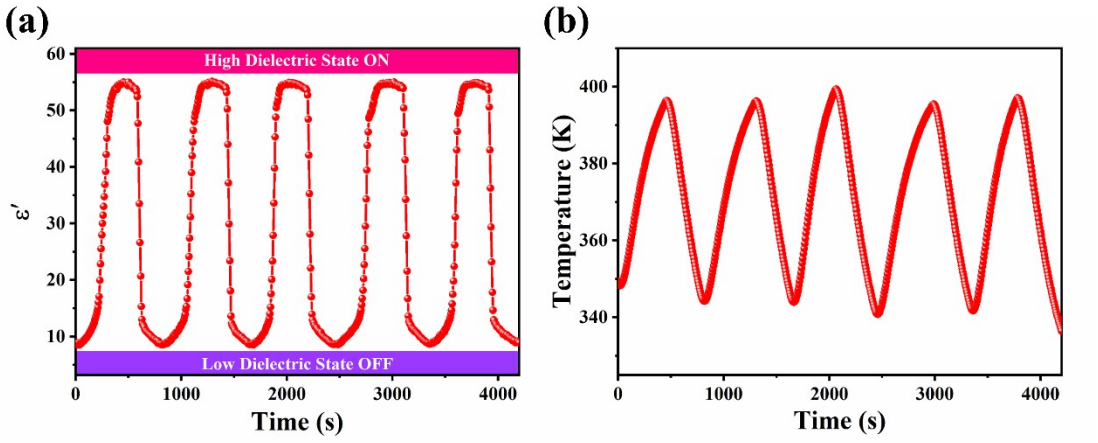

Fig. S7 (a) Dielectric switch-time curve of **1** at 1 MHz measured along the crystallographic *b*-axis. (b) Temperature-time curve corresponding to the dielectric switching measurement.

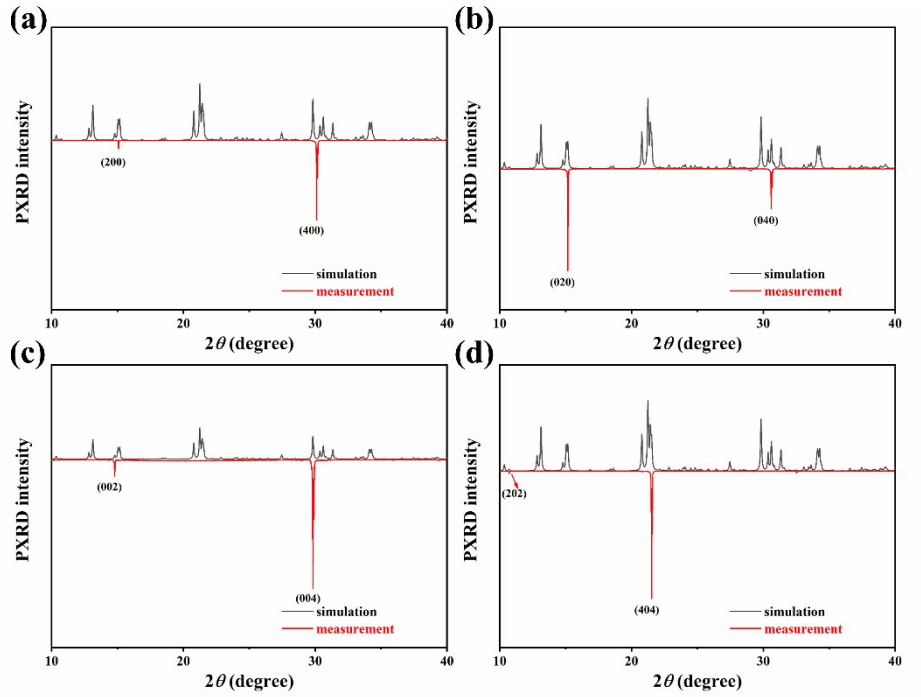

Fig. S8 Measured and simulated PXRD patterns for **1** along the crystallographic *a*-axis, *b*-axis, *c*-axis, and (101) plane.

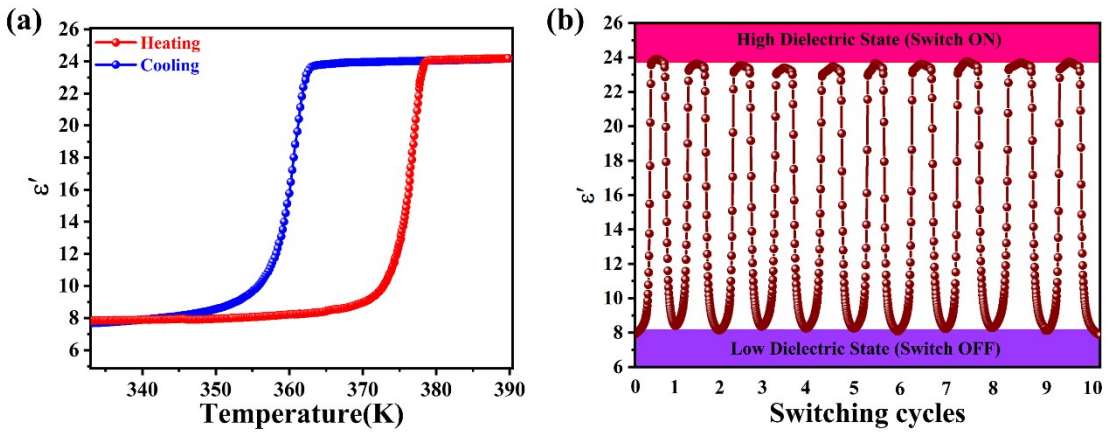

Fig. S9 (a) ε' of the pressed powder pellet of **1** measured at 1 MHz upon heating and cooling process, (b) The dielectric switching cycles of the pressed powder pellet of **1** measured at 1 MHz.

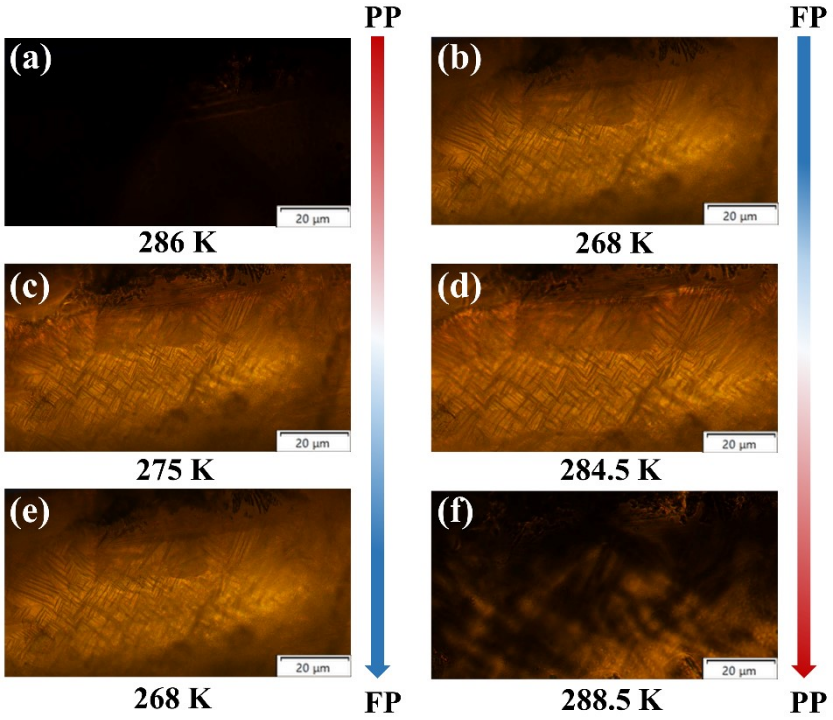

Fig. S10 Evolution of the domain structure of **2** in the heating-cooling cycle.

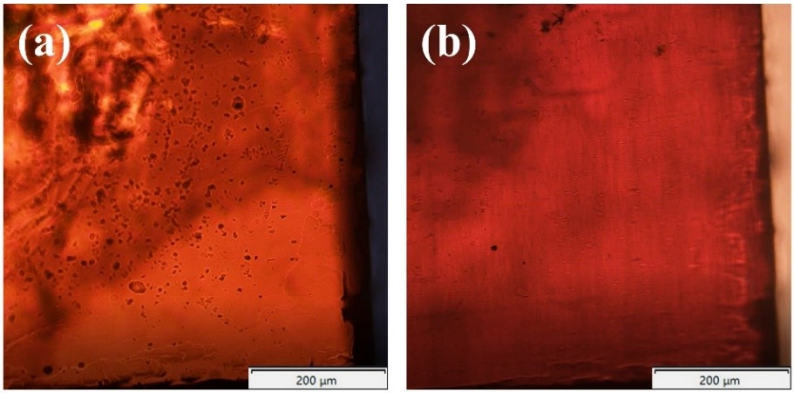

Fig. S11 The morphology of the crystal of **1**. (a) initial state, (b) after the heating and cooling process.

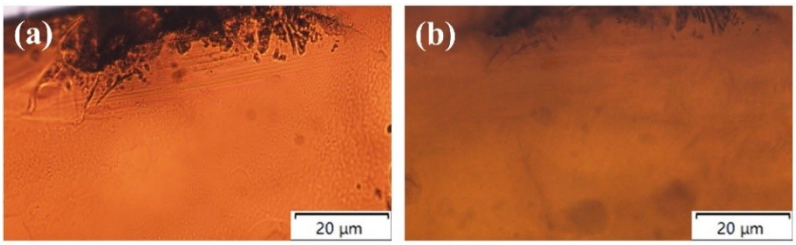

Fig. S12 The morphology of the crystal of **2**. (a) initial state, (b) after the heating and cooling process.

Table S1. Crystal data, data collection, and reduction parameters of **1** and **2**.

Compound	**1**		**2**	
Formula	$C_{10}H_{16}FeKN_8O_2$	$C_{10}H_{16}FeKN_8O_2$	$C_{10}H_{16}FeKN_8$	$C_{10}H_{16}FeKN_8$
Weight	375.26	375.26	343.26	343.26
Temperature	300 K	403 K	243 K	300 K
System	Monoclinic	Cubic	Monoclinic	Cubic
Space group	$P2_1/n$	$Fm\bar{3}m$	$P2_1/n$	$Fm\bar{3}m$
a (Å)	11.7710(3)	11.9312(5)	7.9025(6)	11.7803(1)
b (Å)	11.6695(3)	11.9312(5)	8.5039(7)	11.7803(1)
c (Å)	11.9739(3)	11.9312(5)	11.9308(10)	11.7803(1)
α (°)	90	90	90	90
β (°)	91.999(2)	90	91.407(7)	90
γ (°)	90	90	90	90
V (Å^3)	1643.75(7)	1698.5(2)	801.53(11)	1634.82(4)
Z	4	2	2	2
R_1	0.0467	0.0367	0.1066	0.0166
wR_2	0.1363	0.0932	0.2628	0.0454
GOF	1.024	1.165	1.004	1.081

Table S2. A summary of phase transition temperature and the change of dielectric constant of some cyano-bridged bimetallic complexes.

Materials	Δε′	T_c/K	Reference
$[C(NH_2)_3]_2[KFe(CN)_6]$	1	439	[1]
$[CH(NH_2)_2]_2[KCo(CN)_6]$	1.1	321	[2]
$[CH(NH_2)_2]_2[KFe(CN)_6]$	1.5	321	[2]
$(CH_3NH_3)_2[KCo(CN)_6]$	14	421	[3, 4]
$(CH_3NH_3)_2[KCr(CN)_6]$	15	447	[5]
$(CH_3NH_3)_2[RbCo(CN)_6]$	14	485	[4]
$(CH_3NH_3)_2[KFe(CN)_6]$	10	429	[3, 6]
$[(CH_3)_2NH_2]_2[KCr(CN)_6]$	23	481	[7]
$[(CH_3)_2NH_2]_2[KFe(CN)_6]$	13	226	[6]
$[(CH_3)_3NH]_2[KCo(CN)_6]$	3	350	[8]
$[(CH_3)_3NH]_2[KFe(CN)_6]$	2.5	316	[6, 8]
$[CH_3C(NH_2)_2]_2[KCr(CN)_6]$	10	343	[9]
$[CH_3C(NH_2)_2]_2[KCo(CN)_6]$	7	388	[9]
$(imidazolium)_2[RbCo(CN)_6]$	22	229	[10]
$(azetidinium)_2(H_3O)[Co(CN)_6]$	3	300	[11]
$(pyrrolidinium)_2KCr(CN)_6$	38.5	238	[12]
$(CH_3)(H_2O)[Sr(H_2O)_2Co(CN)_6]$	20	180	[13]
$(HIm)_2[KFe(CN)_6]$	20	187	[14]
$[(CH_3)_4N]_2[KFe(CN)_6]$	0	350	[6]
$(CH_3NH_3)_2[NaCo(CN)_6]$	18	260	[4]
$(imidazolium)_2[KCo(CN)_6]$	18	198	[15]
$[C_3H_4NS]_2[KCo(CN)_6]$	3.5	210	[16]
$[(CH_3)_2NH_2]_2[KCo(CN)_6]$	15	245	[17]
$(azetidinium)_2[KCr(CN)_6]$	22	174	[18]
$(azetidinium)_2[KFe(CN)_6]$	32	188	[18]
$[azetidinium]_2[KCo(CN)_6]$	11	199	[19]
$[(CH_3)_3NCH_2F]_2[KFe(CN)_6]$	2.5	253	[20]
$[(CH_3)_3NOH]_2[KFe(CN)_6]$	12	402	[21, 22]
$[(CH_3)_3NOH]_2[KCo(CN)_6]$	3	417	[21, 23]
$[(CH_3)_3NNH_2]_2[Co(CN)_6Na(H_2O)]$	2.5	300	[24]
$[CH_3C(NH_2)_2]_2[KFe(CN)_6]$	8	385	[9]
$(pyrrolidinium)_2[KFe(CN)_6]$	6.6	354	[25]
$(pyrrolidinium)_2[KCo(CN)_6]$	7.4	368	[25]
$(OHCH_2CH_2NH_3)_2[KFe(CN)_6]$	45	376	this work

References:

1 W. J. Xu, K. P. Xie, Z. F. Xiao, W. X. Zhang and X. M. Chen, *Cryst. Growth Des.*, 2016, **16**, 7212-7217.

2 M. Trzebiatowska, A. Gągor, L. Macalik, P. Peksa and A. Sieradzki, *Dalton Trans.*, 2019, **48**, 15830-15840.

3 M. Rok, J. K. Prytys, V. Kinzhybalo and G. Bator, *Dalton Trans.*, 2017, **46**, 2322-2331.

4 C. Shi, C. H. Yu and W. Zhang, *Angew. Chem.*, 2016, **55**, 5798-5802.
5 M. Rok, M. Moskwa, M. Działowa, A. Bieńko, C. Rajnak, R. Boča and G. Bator, *Dalton Trans.*, 2019, **48**, 16650-16660.
6 W. J. Xu, S. L. Chen, Z. T. Hu, R. B. Lin, Y. J. Su, W. X. Zhang and X. M. Chen, *Dalton Trans.*, 2016, **45**, 4224-4229.
7 M. Rok, G. Bator, B. Zarychta, B. Dziuk, J. Repeć, W. Medycki, M. Zamponi, G. Usevičius, M. Šimėnas and J. Banys, *Dalton Trans.*, 2019, **48**, 4190-4202.
8 M. Rok, B. Zarychta, M. Moskwa, B. Dziuk, W. Medycki and G. Bator, *Dalton Trans.*, 2020, **49**, 1830-1838.
9 M. Rok, G. Bator, B. Zarychta, B. Dziuk, D. K. Skałecki, W. Medycki and M. Zamponi, *Cryst. Growth Des.*, 2019, **19**, 4526-4537.
10 C. Shi, Z. X. Gong, Q. W. Wang, X. B. Han and W. Zhang, *CrystEngComm*, 2020, **22**, 1848-1852.
11 M. Moskwa, P. Sobieszczyk, J. W. Mikurenda, P. Zieliński and M. Rok, *Chem. Commun.*, 2023, **59**, 5535-5538.
12 M. Mączka, A. Nowok, J. K. Zaręba, D. Stefańska, A. Gągor, M. Trzebiatowska and A. Sieradzki, *ACS Appl. Mater. Interfaces*, 2022, **14**, 1460-1471.
13 Y. L. Liu and W. Zhang, *Chem. Commun.*, 2017, **53**, 6077-6080.
14 W. Zhang, Y. Cai, R. G. Xiong, H. Yoshikawa and K. Awaga, *Angew. Chem. Int. Ed.*, 2010, **49**, 6608-6610.
15 X. Zhang, X. D. Shao, S. C. Li, Y. Cai, Y. F. Yao, R. G. Xiong and W. Zhang, *Chem. Commun.*, 2015, **51**, 4568-4571.
16 Z. X. Gong, Q. W. Wang, J. J. Ma, J. Y. Jiang, D. Y. E, Z. Q. Li, F. W. Qi and H. Liang, *Mater. Chem. Front.*, 2020, **4**, 918-923.
17 W. Zhang, H. Y. Ye, R. Graf, H. W. Spiess, Y. F. Yao, R. Q. Zhu and R. G. Xiong, *J. Am. Chem. Soc.*, 2013, **135**, 5230-5233.
18 M. Rok, M. Moskwa, J. Hetmańczyk, Ł. Hetmańczyk and G. Bator, *CrystEngComm*, 2022, **24**, 4932-4939.
19 K. Qian, F. Shao, Z. H. Yan, J. Pang, X. Chen and C. Yang, *CrystEngComm*, 2016, **18**, 7671-7674.
20 X. G. Chen, Z. X. Zhang, Y. L. Zeng, S. Y. Tang and R. G. Xiong, *Chem. Commun.*, 2022, **58**, 3059-3062.
21 M. Rok, A. Ciżman, B. Zarychta, J. K. Zaręba, M. Trzebiatowska, M. Mączka, A. Stroppa, S. Yuan, A. E. Phillips and G. Bator, *J. Mater. Chem. C*, 2020, **8**, 17491-17501.
22 W. J. Xu, P. F. Li, Y. Y. Tang, W. X. Zhang, R. G. Xiong and X. M. Chen, *J. Am. Chem. Soc.*, 2017, **139**, 6369-6375.
23 W. J. Xu, K. Romanyuk, Y. Zeng, A. Ushakov, V. Shur, A. Tselev, W. X. Zhang, X. M. Chen, A. Kholkin and J. Rocha, *J. Mater. Chem. C*, 2021, **9**, 10741-10748.
24 W. J. Xu, Y. Zeng, W. Yuan, W. X. Zhang and X. M. Chen, *Chem. Commun.*, 2020, **56**, 10054-10057.
25 M. Trzebiatowska, M. Maczka, A. Gagor and A. Sieradzki, *Inorg. Chem.*, 2020, **59**, 8855-8863.